ROYAL SOCIETY
OF CHEMISTRY

PAPER

Check for updates

Thermally activated delayed fluorescence emitters with low concentration sensitivity for highly efficient organic light emitting devices†

Xiao-Chun Fan,[a] Kai Wang, [ID] *[a] Cai-Jun Zheng, [ID] *[b] Gao-Le Dai, [ID] [a]
Yi-Zhong Shi,[a] Yan-Qing Li,[a] Jia Yu,[a] Xue-Mei Ou[a] and Xiao-Hong Zhang [ID] *[a]

Thermally activated delayed fluorescence (TADF) emitters normally suffer from serious concentration sensitivity, realizing peak electroluminescence efficiencies with precise control of the doping concentrations, which may hinder their practical applications in organic light emitting devices (OLEDs). In this work, we developed TADF emitter 2′,7′-di(10H-phenoxazin-10-yl)spiro[fluorene-9,9′-thioxanthene]10′,10′-dioxide (**SPFS-PXZ**) based on conventional TADF emitter 10,10′-(sulfonylbis(4,1-phenylene))bis(10H-phenoxazine) (**DPS-PXZ**). By introducing a fluorene group, the molecular rigidity and steric hindrance of **SPFS-PXZ** are improved greatly, which contributes to suppressing the strong π–π stacking tendency between phenoxazine segments and reduces intermolecular interactions. In turn, **SPFS-PXZ** successfully exhibits low concentration sensitivity in OLEDs, and keeps high maximum external quantum efficiencies (EQEs) over 20.8% with a small EQE fluctuation of 2.1% in a wide doping concentration range from 10 wt% to 50 wt%. These results prove that **SPFS-PXZ** is an ideal model to develop efficient TADF emitters with low concentration sensitivity.

Introduction

Organic light emitting devices (OLEDs) always draw wide attention due to their great potential in displays and lighting.[1,2] In devices, only 25% of excitons are electro-generated in the singlet state according to the spin statistics rule, thus the 75% of triplet excitons will be wasted for traditional fluorescent emitters.[3] Although phosphorescent emitters can utilize both singlet and triplet excitons, the high cost of noble metals limits their practical application.[4–6] As a result, pure organic thermally activated delayed fluorescence (TADF) emitters are considered to be the best candidates as the emitters of OLEDs, since they can theoretically achieve 100% internal quantum efficiency *via* an efficient reverse intersystem crossing (RISC) process from the lowest triplet state (T$_1$) to the lowest singlet state (S$_1$) at room temperature.[7]

To achieve an efficient RISC process, the singlet–triplet splittings (ΔE_{ST}s) between the S$_1$ and T$_1$ states must be limited to extremely small values, which can only be realized by minimizing the overlap between the highest occupied molecular orbital (HOMO) and the lowest occupied molecular orbital (LUMO).[8] Therefore, linking electron donor (D) and electron acceptor (A) moieties with a twisted structure has become the most common and effective method to construct TADF emitters, as the HOMO and LUMO can be separately distributed in D and A moieties in these D–A frameworks. With various D and A segments, a large number of efficient TADF emitters have been developed in the past few years,[9–38] and the optimized OLEDs based on these TADF emitters have realized extremely high maximum external quantum efficiencies (EQEs) over 30%, demonstrating their promising future. However, current TADF emitters normally suffer from serious concentration sensitivity in the OLEDs. With enough doping concentration to harvest all excitons on the host, most of the TADF emitters fall into trouble with significant concentration quenching. Therefore, the peak efficiencies of the OLEDs based on these TADF emitters can only be achieved with precise control of the doping concentrations, which are usually lower than 15 wt%.[39] However, during practical manufacturing, uniform and reproducible control over doping concentrations is hardly achieved especially with low values, resulting in unstable performance and high cost of commercial products. Furthermore, according to Zhang *et al.*'s report, high doping concentrations of TADF emitters could also benefit in realizing more balanced charge transport

[a] *Institute of Functional Nano & Soft Materials (FUNSOM), Jiangsu Key Laboratory for Carbon-Based Functional Materials & Devices, Soochow University, Suzhou, Jiangsu, 215123, P. R. China. E-mail: xiaohong_zhang@suda.edu.cn, wkai@suda.edu.cn*

[b] *School of Optoelectronic Science and Engineering, University of Electronic Science and Technology of China, Chengdu, Sichuan, 610054, P. R. China. E-mail: zhengcaijun@uestc.edu.cn*

† Electronic supplementary information (ESI) available: Cyclic voltammetry, TGA and DSC thermograms, and EL performances. See DOI: 10.1039/c9tc02032b

This journal is © The Royal Society of Chemistry 2019

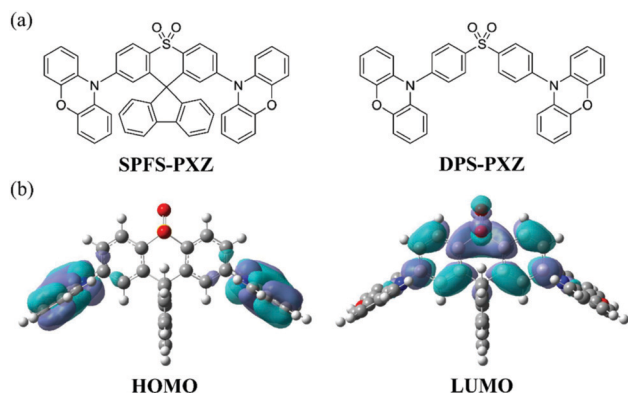*J. Mater. Chem. C*, 2019, 7, 8923–8928 | 8923

Fig. 1 (a) Molecular structure of **SPFS-PXZ** and **DPS-PXZ**. (b) HOMO and LUMO spatial distributions of **SPFS-PXZ**.

and a wider charge recombination zone, and thus significantly improve the stability of the devices.[40] Therefore, it is highly desired to develop TADF emitters with low concentration sensitivity, keeping peak efficiencies within a wide doping concentration range.

As reported by Takuma Yasuda *et al.* in 2017, concentration quenching of TADF molecules was dominated by electron-exchange interactions for long-lived triplet excitons, and was quite sensitive with the intermolecular distances.[23] Since lots of employed D and A moieties in TADF emitters, like carbazole, phenothiazine (PXZ), and anthraquinone, have planar structures to realize highly twisted structures, their derivatives suffer from strong π–π stacking tendency between these planar segments, resulting in serious concentration quenching behaviors. In this work, taking the reported TADF emitter 10,10′-(sulfonyl bis(4,1-phenylene))bis(10*H*-phenoxazine) (**DPS-PXZ**) as the original, we designed and synthesized optimized TADF emitter 2′,7′-di(10*H*-phenoxazin-10-yl)spiro[fluorene-9,9′-thioxanthene]-10′,10′-dioxide (**SPFS-PXZ**) as shown in Fig. 1.[22,40,41] Due to strong π–π stacking tendency between PXZ segments, **DPS-PXZ** exhibits high concentration-sensitivity. By introducing a fluorene group into the sulfonyldibenzene (DPS) moiety, the rigidity of the modified A component spiro[fluorene-9,9′-thioxanthene]-10′,10′-dioxide (SPFS) is evidently enhanced, which will restrict

the molecular relaxation of **SPFS-PXZ** and improve its photoluminescence quantum yield (PLQY). Moreover, compared with **DPS-PXZ**, intermolecular steric hindrance of **SPFS-PXZ** is significantly improved, resulting in suppressed concentration quenching and much lower concentration sensitivity. As expected, the optimized OLED based on **SPFS-PXZ** realizes excellent performance with a maximum EQE, current efficiency (CE) and power efficiency (PE) of 22.9%, 64.9 cd A^{-1} and 65.7 lm W^{-1}, respectively, which is superior to the corresponding **DPS-PXZ**-based devices. More importantly, with doping concentration gradually increasing from 10 wt% to 50 wt%, **SPFS-PXZ**-based devices exhibit stable EQEs with a small fluctuation of 2.1%. These results prove that **SPFS-PXZ** is the ideal model to develop efficient TADF emitters with low concentration sensitivity.

Results and discussion

Synthesis and characterization

SPFS-PXZ was obtained using a simple and efficient synthetic route with a high yield as shown in Scheme 1. Intermediate **3** was prepared *via* the carbonyl addition reaction involving *n*-butyllithium (*n*-BuLi) with 2,7-dibromo-9*H*-thioxanthen-9-one (**1**) and 2-bromo-1,1′-biphenyl (**2**). Then intermediate **3** was further subjected to dehydration ring-closure reactions and oxidation reactions to obtain 2′,7′-dibromospiro[fluorene-9,9′-thioxanthene]10′,10′-dioxide (**5**). Finally, the target compound **SPFS-PXZ** was synthesized *via* the Buchwald–Hartwig reaction involving **5** and PXZ. Nuclear magnetic resonance (NMR) spectroscopy and mass spectrometry were fully characterized to confirm the chemical structures of the intermediates and the target compound.

Thermal properties

The thermodynamic analysis was characterized by thermogravimetric analysis (TGA) and differential scanning calorimetry (DSC) measurements. From TGA and DSC curves (shown in Fig. S1, ESI†), **SPFS-PXZ** exhibits high thermal stability with a decomposition temperature (T_d, defined as the temperature of 5% weight loss) of 445 °C, slightly higher than that of **DPS-PXZ**. Moreover, in
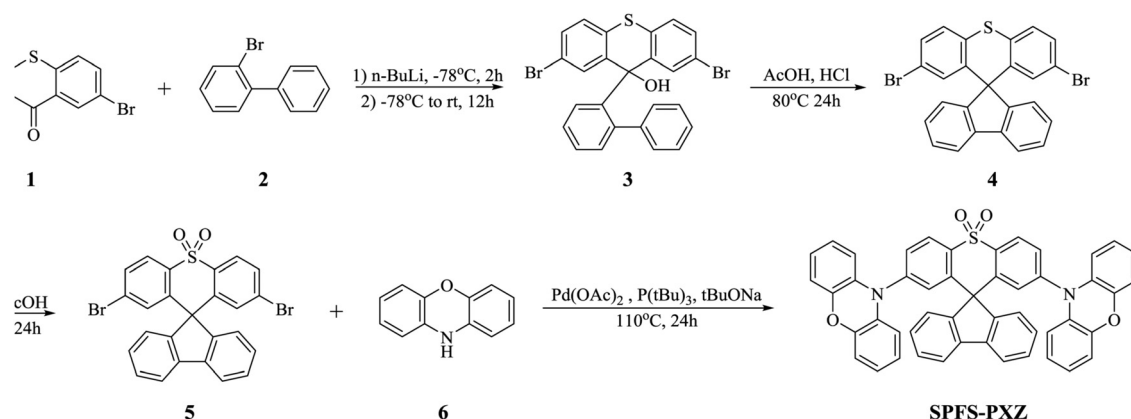
Scheme 1 Synthesis route to **SPFS-PXZ**.

the measurement range from 25 to 200 °C, no distinct glass transition can be observed from the DSC curve. This result guarantees its high thermal stability for OLED applications.

Theoretical calculations and electrochemical properties

To give an in-depth explanation on the spatial distributions of frontier molecular orbitals (FMOs), time-dependent density function theory (TD-DFT) calculations were carried out on **SPFS-PXZ** in the ground state (S_0) using the B3LYP/6-31g(d) basis set in the Gaussian 09 program package. As shown in Fig. 1, benefitting from the nearly perpendicular dihedral angles between PXZ and SPFS moieties, an obvious FMO separation is achieved with the HOMO mainly locating on PXZ moieties and the LUMO mainly locating on the SPFS moiety. Specifically, since the spiral carbon atom breaks the conjugation between DPS and fluorene, there is barely any LUMO distribution observed on the fluorene group, suggesting that the additional fluorene group has no influence on the FMO distributions. As expected, ΔE_{ST} of **SPFS-PXZ** is calculated to be 0.02 eV by using the optimal HF exchange method (listed in Table S1, ESI†).[41] Such a small ΔE_{ST} value would ensure an effective RISC process, thus resulting in TADF characteristics. Moreover, compared with **DPS-PXZ**, **SPFS-PXZ** has a more rigid and sterically hindered molecular structure due to the additional restriction from the fluorene group. Thus, it can be expected that the non-radiative process of **SPFS-PXZ** will be further suppressed, resulting in a higher PLQY than **DPS-PXZ**.

The electrochemical property of **SPFS-PXZ** was investigated by performing cyclic voltammetry (CV) measurements. As shown in Fig. S3 (ESI†), from the onset positions of oxidation and reduction curves with respect to that of ferrocene, the HOMO and LUMO energy levels of **SPFS-PXZ** were estimated to be −5.39 and −2.79 eV, respectively. As listed in Table 1, the HOMO value of **SPFS-PXZ** is identical to that of **DPS-PXZ**, which can be ascribed to the same employed D moiety, whereas its LUMO energy level is slightly shallower than that of **DPS-PXZ** (−2.88 eV), which should be attributed to the low electron-donating ability of the additional fluorene group. Accordingly, the electrochemical band gaps of **SPFS-PXZ** and **DPS-PXZ** are calculated to be 2.60 and 2.51 eV, respectively.

Photophysical properties

The photophysical properties of **SPFS-PXZ** were then fully characterized. Fig. 2a shows the UV-Vis absorption spectrum of **SPFS-PXZ** in toluene at room temperature. Due to the similar skeleton, **SPFS-PXZ** exhibits a similar absorption range and shape to **DPS-PXZ** (shown in Fig. S4, ESI†). The absorption
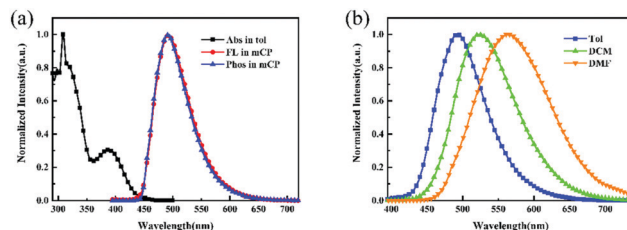

Fig. 2 (a) UV-vis absorption spectrum of **SPFS-PXZ** (black) in toluene at room temperature, the fluorescence spectrum (red) and the phosphorescence spectrum (blue) of **SPFS-PXZ** (30 wt% doped in mCP films) at 77 K. (b) Fluorescence spectra of **SPFS-PXZ** in different polar solvents: toluene (blue), dichloromethane (green), and dimethyl formamide (orange).

below 340 nm could be attributed to the π–π* transition of the high-lying local excited state, while the structureless absorption band around 390 nm should be assigned to the intramolecular charge-transfer (ICT) transition from the PXZ moiety to the SPFS moiety. As shown in Fig. 2b, in toluene at room temperature, **SPFS-PXZ** shows bluish-green emission with a peak at 492 nm, which is slightly shorter than that of **DPS-PXZ** (λ_{max} = 507 nm) and consistent with its slightly broader bandgap estimated by the CV measurement.

To further confirm its ICT characteristic, fluorescence spectra of **SPFS-PXZ** were measured in different solvents from initial low polar toluene to high polar dichloromethane (DCM) and N,N-dimethylformamide (DMF). As shown in Fig. 2b, fluorescence spectra undergo a significant red-shift from an initial peak at 492 nm in toluene to 524 nm in DCM and 563 nm in DMF, respectively, indicating significant ICT characteristics of **SPFS-PXZ**. As summarized in Table S2 (ESI†), the Stokes shift and FWHM of **SPFS-PXZ** are smaller than the corresponding parameters of **DPS-PXZ**, suggesting that the solvatochromic effect of **SPFS-PXZ** was relatively suppressed, which should be attributed to the more rigid structure of **SPFS-PXZ** further suppressing the molecular relaxation process. Fig. 2a also illustrates the fluorescence and phosphorescence spectra of 30 wt% **SPFS-PXZ** doped in 1,3-di(9H-carbazol-9-yl)benzene (mCP) films at 77 K. From the onset positions of the fluorescence (λ_{on} = 445 nm) and phosphorescence (λ_{on} = 447 nm) spectra, the energy levels of S_1 and T_1 states are calculated to be 2.789 and 2.776 eV respectively. Thus, an extremely small ΔE_{ST} of 0.013 eV is estimated for **SPFS-PXZ**, well consistent with our theoretical prediction, suggesting its potential TADF feature.

In the previous report, **DPS-PXZ** is confirmed to exhibit an aggregation-induced emission (AIE) phenomenon. Herein, to explore the influence of introducing steric hindrance on the AIE

Table 1 Photophysical parameters of **SPFS-PXZ** and **DPS-PXZ**

Compound	$\lambda_{abs}{}^a$ [nm]	$\lambda_{em}{}^b$ [nm]	$S_1{}^c/T_1{}^c$ [eV]	HOMO/LUMO^d [eV]	$\Delta E_{ST}{}^e$ [eV]	PLQY^f [%]
SPFS-PXZ	390	492	2.79/2.78	−5.39/−2.79	0.013	55.9^g/72.3^h/60.3^i
DPS-PXZ	390	507	2.89/2.73	−5.39/−2.88	0.081	51.5^g/40.9^h/32.3^i

^{a} Maximum wavelength of the UV-vis absorption spectrum. ^{b} Maximum wavelength of the fluorescence spectrum measured in toluene at room temperature. ^{c} The energy levels of S_1 and T_1 estimated from the onset position of the fluorescence and phosphorescence spectra of doping in mCP films at 77 K. ^{d} Measured in DMF at room temperature. ^{e} Calculated from the equation: $\Delta E_{ST} = S_1 - T_1$. ^{f} The photoluminescence quantum yield of **SPFS-PXZ** and **DPS-PXZ** doped in mCP films. ^{g} 10 wt%. ^{h} 30 wt%. ^{i} 50 wt%.

feature, we measured the emission behaviors of **SPFX-PXZ** in tetrahydrofuran (THF)/water mixtures with different water fractions. As shown in Fig. S5 (ESI†), a significant AIE phenomenon was observed, suggesting that **SPFX-PXZ** is also an AIE TADF emitter, which is beneficial to realize a high PLQY under high doping concentration.

The transition PL decays of **SPFS-PXZ** were carried out at room temperature. As shown in Fig. 3, **SPFS-PXZ**-doped mCP films with doping concentrations from 10 wt% to 50 wt% all exhibit two distinct lifetimes with a prompt component at a nanosecond order of magnitude and a delay component at a microsecond order of magnitude, corresponding to the prompt fluorescence and the delayed fluorescence, respectively. The existence of the delayed fluorescence confirms the TADF characteristic of **SPFS-PXZ**. Moreover, with increased doping concentration, the **SPFS-PXZ**-doped films only show a slight change in transition PL decay curves; while for **DPS-PXZ**-doped ones, the decrease becomes more evident. These results confirmed that the introduction of the fluorene group in **SPFS-PXZ** further suppresses concentration quenching evidently, beneficial to realizing stable exciton utilization in a wide doping concentration range.

To further confirm their different concentration sensitivity, the PLQYs of **SPFS-PXZ** and **DPS-PXZ** doped mCP films were measured with various doping concentrations at room temperature. As summarized in Table 1, with doping concentrations from 10 wt% to 30 wt% and 50 wt%, **SPFS-PXZ**-doped films show high PLQYs of 55.9%, 72.3% and 60.3%, respectively, while under the same conditions, **DPS-PXZ**-doped films exhibit a sharp PLQY decline from 51.5% to 40.9% and 32.3%. The PLQY values of **SPFS-PXZ** are all evidently higher than that of **DPS-PXZ**, which should be ascribed to the reduced molecular relaxation. More importantly, compared with **DPS-PXZ**, the concentration sensitivity of **SPFS-PXZ** is significantly suppressed, because the large steric hindrance of the fluorene group breaks the strong π–π interactions of PXZ segments and reduces intermolecular interaction between **SPFS-PXZ** molecules.

OLED devices

Finally, to compare the electroluminescence (EL) performance of **SPFS-PXZ** and **DPS-PXZ**, the OLEDs using **SPFS-PXZ** and **DPS-PXZ** as emitters were finally fabricated with an identical architecture of ITO/TAPC (30 nm)/TCTA (10 nm)/mCP: x wt% **SPFS-PXZ** or **DPS-PXZ** (20 nm)/TmPyPb (40 nm)/LiF (1 nm)/Al, where ITO (indium tin oxide), TAPC (4,4′-(cyclohexane-1,1-diyl)bis(N,N-di-p-tolylaniline)),

TCTA (tris(4-(9H-carbazol-9-yl)phenyl)amine), TmPyPb (1,3,5-tri-[(32pyridyl)-phen-3-yl]benzene), LiF and Al act as the anode, hole-injection, hole-transporting, electron-transporting, electron-injection and cathode layers, respectively. The energy level diagram and molecular structures of the used materials in the devices are shown in Fig. 4a and Fig. S9 (ESI†), respectively. According to the HOMO and LUMO energy levels of **SPFS-PXZ**, mCP was chosen as the optimal host matrix to balance the carrier recombination. And a series of devices with the doping concentration varying from 10 wt% to 50 wt% were fabricated to investigate the concentration sensitivity of **SPFS-PXZ** and **DPS-PXZ** in detail.

Table 2 summarizes the key performance of **SPFS-PXZ** and **DPS-PXZ** based devices. All the devices exhibit low turn-on voltages (V_{on}) of ~ 3.0 V (defined voltage at 10 cd m^{-2}). In particular, with the doping concentration gradually increasing from 10 wt% to 50 wt%, the V_{on}s evidently decline for both emitters, which should be assigned to the direct charge trap of emitters. Meanwhile, as shown in Fig. 4b and Fig. S6 (ESI†), with doping ratios gradually increased, both EL spectra underwent a slight red-shift as well, from 504 to 516 nm for **SPFS-PXZ** and from 516 to 532 nm for **DPS-PXZ**, respectively. This is because **SPFS-PXZ** and **DPS-PXZ** molecules can also increase the
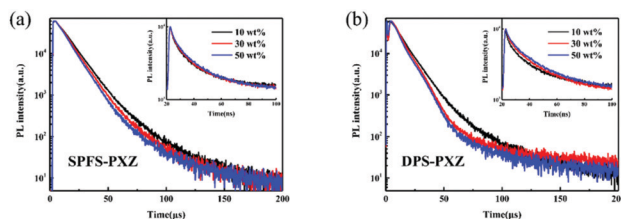

Fig. 4 (a) Energy level diagram of **SPFS-PXZ**-doped and **DPS-PXZ**-doped devices. (b) EL spectra at 1000 cd m^{-2}, (c) luminance−external quantum efficiency and (d) voltage−luminance−current density characteristics of **SPFS-PXZ**-doped devices for different doping concentrations: black (10 wt% doped in mCP), red (30 wt% doped in mCP), and blue (50 wt% doped in mCP). (e) Effect of maximum external quantum efficiency−doping concentration on mCP characteristics of **SPFS-PXZ** (black) and **DPS-PXZ** (red) based OLEDs.

Fig. 3 Transient PL decay curves of **SPFS-PXZ** (a) and **DPS-PXZ** (b) doped in mCP films at different doping concentrations (black-10 wt%, red-30 wt%, and blue-50 wt%) within a time period of micro- and nanoseconds (insets).
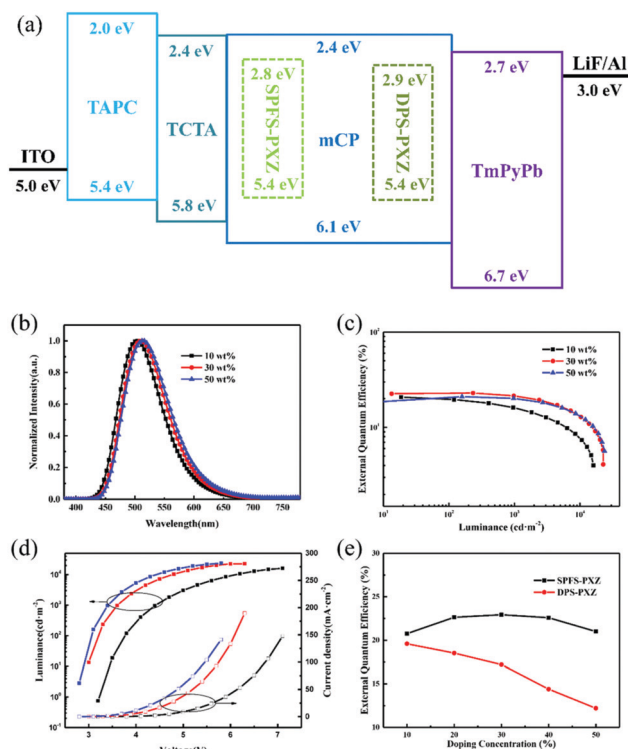
8926 | *J. Mater. Chem. C*, 2019, **7**, 8923–8928

This journal is © The Royal Society of Chemistry 2019

Table 2 EL performance of **SPFS-PXZ**-doped and **DPS-PXZ**-doped devices with different concentrations

Compound	Doping concentration[a] [wt%]	V_{on}[b] [V]	Peak [nm]	Maximum CE/PE/EQE[c] [cd A^{-1}/lm W^{-1}/%]	CIE (x, y)
SPFS-PXZ	10	3.2	504	56.2/53.8/20.8	(0.22, 0.47)
	30	2.9	512	66.8/68.7/22.9	(0.25, 0.52)
	50	2.8	516	62.5/63.3/21.0	(0.27, 0.54)
DPS-PXZ	10	3.0	516	61.4/63.1/19.3	(0.28, 0.56)
	30	2.7	524	58.0/60.7/17.2	(0.31, 0.28)
	50	2.6	532	40.9/41.4/12.2	(0.35, 0.58)

[a] Doping concentration in mCP. [b] Turn-on voltage defined at 10 cd m^{-2}. [c] CE: current efficiency, PE: power efficiency, EQE: external quantum efficiency.

polarity of the EML, thus causing solvatochromaticity like in solutions.

Fig. 4c and Fig. S8 (ESI†) illustrate the luminance–EQE curves of these devices. The optimized OLED based on **SPFS-PXZ** exhibits the maximum EQE, CE and PE estimated up to 22.9%, 64.9 cd A^{-1} and 65.7 lm W^{-1}, respectively, which are evidently higher than the optimized results of **DPS-PXZ**-doped devices (19.3%, 61.4 cd A^{-1} and 63.1 lm W^{-1}), suggesting the higher exciton utilization of **SPFS-PXZ**. Moreover, at a luminance of 1000 cd m^{-2}, the EQE still remained a high value of 21.5%, corresponding to an extremely small roll-off of only 6.1%, suggesting the superior exciton utilization under high current density. Intriguingly, the two emitters exhibit different variation trends with increased doping concentrations in the OLEDs. For **DPS-PXZ**, the best efficiency is achieved at a common doping concentration of 10 wt%, while with further increased doping concentration, **DPS-PXZ**-based devices suffer a sharp efficiency decline to a maximum EQE of only 12.2% at a doping concentration of 50 wt%. Such a high concentration sensitivity is similar with most reported TADF emitters, which should be attributed to the strong π–π interactions of PXZ segments which leads to serious concentration quenching. Correspondingly, as large steric hindrance of an additional fluorene group suppresses the π–π interactions of PXZ units, and **SPFS-PXZ** reaches its optimized device performance at a high doping concentration of 30 wt%. Moreover, in a wide doping concentration range from 10 wt% to 50 wt%, **SPFS-PXZ**-based devices all possess high maximum EQEs of over 20.8%. Such a small EQE fluctuation of 2.1% is significantly smaller than **DPS-PXZ**, indicating the superior low concentration sensitivity of **SPFS-PXZ**.

Conclusions

In summary, to suppress annoying concentration quenching, we proposed a simple strategy by introducing extra steric hindrance to develop TADF emitters with low concentration sensitivity. Accordingly, optimized TADF emitter **SPFS-PXZ** was developed based on the reported TADF emitter **DPS-PXZ**. The additional fluorene framework restricts the molecular relaxation, resulting in an improved PLQY. Moreover, the large steric hindrance of the fluorene group can evidently suppress the strong π–π stacking tendency of PXZ segments for **SPFS-PXZ**, thus reducing concentration sensitivity. In the OLEDs, **SPFS-PXZ** exhibits excellent performance with peak EQE, CE, and PE of

22.9%, 64.9 cd A^{-1} and 65.7 lm W^{-1} and a small efficiency roll-off of only 6.1% at a high luminance of 1000 cd m^{-2}. More importantly, in a wide doping concentration range from 10 wt% to 50 wt%, **SPFS-PXZ**-based OLEDs exhibit an extremely small EQE fluctuation of 2.1%, proving its superior low concentration sensitivity. We believed that such a practice could act as a simple strategy to develop TADF emitters with low concentration sensitivity.

Conflicts of interest

There are no conflicts to declare.

Acknowledgements

Notes and references

1 C. W. Tang and S. A. VanSlyke, *Appl. Phys. Lett.*, 1987, **51**, 913–915.
2 M. A. Baldo, D. F. O'Brien, Y. You, A. Shoustikov, S. Sibley, M. E. Thompson and S. R. Forrest, *Nature*, 1998, **395**, 151–154.
3 M. A. Baldo, D. F. O'Brien, M. E. Thompson and S. R. Forrest, *Phys. Rev. B: Condens. Matter Mater. Phys.*, 1999, **60**, 14422–14428.
4 C. Adachi, M. A. Baldo, M. E. Thompson and S. R. Forrest, *J. Appl. Phys.*, 2001, **90**, 5048–5051.
5 S. J. Su, H. Sasabe, Y. J. Pu, K. Nakayama and J. Kido, *Adv. Mater.*, 2010, **22**, 3311–3316.
6 C. W. Lee and J. Y. Lee, *Adv. Mater.*, 2013, **25**, 5450–5454.
7 H. Uoyama, K. Goushi, K. Shizu, H. Nomura and C. Adachi, *Nature*, 2012, **492**, 234–238.
8 S. Hirata, Y. Sakai, K. Masui, H. Tanaka, S. Y. Lee, H. Nomura, N. Nakamura, M. Yasumatsu, H. Nakanotani,

Q. Zhang, K. Shizu, H. Miyazaki and C. Adachi, *Nat. Mater.*, 2015, **14**, 330–336.

9 Q. Zhang, J. Li, K. Shizu, S. Huang, S. Hirata, H. Miyazaki and C. Adachi, *J. Am. Chem. Soc.*, 2012, **134**, 14706–14709.

10 X. K. Liu, Z. Chen, C. J. Zheng, C. L. Liu, C. S. Lee, F. Li, X. M. Ou and X. H. Zhang, *Adv. Mater.*, 2015, **27**, 2378–2383.

11 J. X. Chen, K. Wang, C. J. Zheng, M. Zhang, Y. Z. Shi, S. L. Tao, H. Lin, W. Liu, W. W. Tao, X. M. Ou and X. H. Zhang, *Adv. Sci.*, 2018, **5**, 1800436.

12 F. B. Dias, K. N. Bourdakos, V. Jankus, K. C. Moss, K. T. Kamtekar, V. Bhalla, J. Santos, M. R. Bryce and A. P. Monkman, *Adv. Mater.*, 2013, **25**, 3707–3714.

13 L. Gan, K. Gao, X. Cai, D. Chen and S.-J. Su, *J. Phys. Chem. Lett.*, 2018, **9**, 4725–4731.

14 M. Li, C.-F. Chen, M. Li, C.-F. Chen, S.-H. Li, M.-K. Fung, D. Zhang, M. Cai and L. Duan, *Angew. Chem., Int. Ed.*, 2018, **57**, 2889–2893.

15 X.-L. Li, G. Xie, M. Liu, D. Chen, X. Cai, J. Peng, Y. Cao and S.-J. Su, *Adv. Mater.*, 2016, **28**, 4614–4619.

16 W. Liu, J.-X. Chen, C.-J. Zheng, K. Wang, D.-Y. Chen, F. Li, Y.-P. Dong, C.-S. Lee, X.-M. Ou and X.-H. Zhang, *Adv. Funct. Mater.*, 2016, **26**, 2002–2008.

17 X. K. Liu, Z. Chen, C. J. Zheng, M. Chen, W. Liu, X. H. Zhang and C. S. Lee, *Adv. Mater.*, 2015, **27**, 2025–2030.

18 Y. Z. Shi, K. Wang, X. Li, G. L. Dai, W. Liu, K. Ke, M. Zhang, S. L. Tao, C. J. Zheng, X. M. Ou and X. H. Zhang, *Angew. Chem., Int. Ed.*, 2018, **57**, 9480–9484.

19 K. Wang, C. J. Zheng, W. Liu, K. Liang, Y. Z. Shi, S. L. Tao, C. S. Lee, X. M. Ou and X. H. Zhang, *Adv. Mater.*, 2017, **29**, 1701476.

20 W. Zeng, H.-Y. Lai, W.-K. Lee, M. Jiao, Y.-J. Shiu, C. Zhong, S. Gong, T. Zhou, G. Xie, M. Sarma, K.-T. Wong, C.-C. Wu and C. Yang, *Adv. Mater.*, 2018, **30**, 1704961.

21 D. Zhang, M. Cai, Y. Zhang, D. Zhang and L. Duan, *ACS Appl. Mater. Interfaces*, 2015, **7**, 28693–28700.

22 S. Gan, W. Luo, B. He, L. Chen, H. Nie, R. Hu, A. Qin, Z. Zhao and B. Z. Tang, *J. Mater. Chem. C*, 2016, **4**, 3705–3708.

23 J. Lee, N. Aizawa, M. Numata, C. Adachi and T. Yasuda, *Adv. Mater.*, 2017, **29**, 1604856.

24 W. L. Tsai, M. H. Huang, W. K. Lee, Y. J. Hsu, K. C. Pan, Y. H. Huang, H. C. Ting, M. Sarma, Y. Y. Ho, H. C. Hu, C. C. Chen, M. T. Lee, K. T. Wong and C. C. Wu, *Chem. Commun.*, 2015, **51**, 13662–13665.

25 J. Li, T. Nakagawa, Q. Zhang, H. Nomura, H. Miyazaki and C. Adachi, *Adv. Mater.*, 2013, **25**, 3319–3323.

26 L. S. Cui, S. B. Ruan, F. Bencheikh, R. Nagata, L. Zhang, K. Inada, H. Nakanotani, L. S. Liao and C. Adachi, *Nat. Commun.*, 2017, **8**, 2250.

27 W. Liu, C. J. Zheng, K. Wang, M. Zhang, D. Y. Chen, S. L. Tao, F. Li, Y. P. Dong, C. S. Lee, X. M. Ou and X. H. Zhang, *ACS Appl. Mater. Interfaces*, 2016, **8**, 32984–32991.

28 X. Li, Y. Z. Shi, K. Wang, M. Zhang, C. J. Zheng, D. M. Sun, G. L. Dai, X. C. Fan, D. Q. Wang, W. Liu, Y. Q. Li, J. Yu, X. M. Ou, C. Adachi and X. H. Zhang, *ACS Appl. Mater. Interfaces*, 2019, **11**, 13472–13480.

29 W.-W. Tao, K. Wang, J.-X. Chen, Y.-Z. Shi, W. Liu, C.-J. Zheng, Y.-Q. Li, J. Yu, X.-M. Ou and X.-H. Zhang, *J. Mater. Chem. C*, 2019, **7**, 4475–4483.

30 L. Gan, Z. Xu, Z. Wang, B. Li, W. Li, X. Cai, K. Liu, Q. Liang and S. J. Su, *Adv. Funct. Mater.*, 2019, 1808088.

31 M. Cai, D. Zhang, J. Xu, X. Hong, C. Zhao, X. Song, Y. Qiu, H. Kaji and L. Duan, *ACS Appl. Mater. Interfaces*, 2019, **11**, 1096–1108.

32 D.-d. Zhang, K. Suzuki, X.-z. Song, Y. Wada, S. Kubo, L. Duan and H. Kaji, *ACS Appl. Mater. Interfaces*, 2019, **11**, 7192–7198.

33 W. Zeng, C. Zhong, S. Gong, T. Zhou, G. Xie, C. Yang, H.-Y. Lai, W.-K. Lee, M. Jiao, Y.-J. Shiu, C.-C. Wu, M. Sarma and K.-T. Wong, *Adv. Mater.*, 2018, **30**, 1704961.

34 M. Bian, D. Zhang, Y. Wang, Y.-H. Chung, Y. Liu, H. Ting, L. Duan, Z. Chen, Z. Bian, Z. Liu and L. Xiao, *Adv. Funct. Mater.*, 2018, **28**, 1800429.

35 B. Li, Z. Wang, S.-J. Su, F. Guo, Y. Cao and Y. Zhang, *Adv. Opt. Mater.*, 2019, 1801496.

36 W. Li, X. Cai, B. Li, L. Gan, Y. He, K. Liu, D. Chen, S.-J. Su and Y.-C. Wu, *Angew. Chem., Int. Ed.*, 2019, **58**, 582–586.

37 M. Huang, Y. Li, K. Wu, J. Luo, G. Xie, L. Li and C. Yang, *Dyes Pigm.*, 2018, **153**, 92–98.

38 X. Zhou, H. Yang, Z. Chen, S. Gong, Z. Lu and C. Yang, *J. Mater. Chem. C*, 2019, **7**, 6607–6615.

39 M. Y. Wong and E. Zysman-Colman, *Adv. Mater.*, 2017, **29**, 1605444.

40 Q. Zhang, D. Tsang, H. Kuwabara, Y. Hatae, B. Li, T. Takahashi, S. Y. Lee, T. Yasuda and C. Adachi, *Adv. Mater.*, 2015, **27**, 2096–2100.

41 Q. Zhang, B. Li, S. Huang, H. Nomura, H. Tanaka and C. Adachi, *Nat. Photonics*, 2014, **8**, 326–332.

8928 | *J. Mater. Chem. C*, 2019, **7**, 8923–8928

This journal is © The Royal Society of Chemistry 2019